

Data-driven Soliton Manifold Approximations for Dark and Bright Waves: Some Prototypical 1d Case Examples

Su Yang^{*1}, Shaoxuan Chen¹, Wei Zhu², and Panayotis G. Kevrekidis^{1,3,4}

¹Department of Mathematics and Statistics, University of Massachusetts Amherst, Amherst, MA 01003-4515, USA

²School of Mathematics, Georgia Institute of Technology, Atlanta, GA 30332, USA

³Department of Physics, University of Massachusetts Amherst, Amherst, MA 01003-4515, USA

⁴Theoretical Sciences Visiting Program, Okinawa Institute of Science and Technology Graduate University, Onna, 904-0495, Japan

October 16, 2025

Abstract

In this paper, we revisit the investigation of solitary-wave interactions in the nonlinear Schrödinger model, both in the presence and absence of a parabolic trapping potential. While approximate dynamics, based on variational—or similar—methods, governed by a system of ordinary differential equations (ODEs) for both bright and dark-soliton interactions have been well established in the literature based on physical expert considerations, this study focuses on a data-driven approach, the so-called Sparse Identification of Nonlinear Dynamics (SINDy). Accordingly, our purpose is to use PDE time-series of select waveform diagnostics in order to numerically reconstruct such approximate dynamics, without prior knowledge thereof. The purpose is not only to verify the robustness of the dynamical approximated ODEs, but also to shed light on the application of such a data-driven methodology in the study of soliton interactions and to formulate a complementary approach, more reliant on the wealth of PDE data and less so on expert theoretical constructs.

Keywords. Solitons, Data-driven method, Nonlinear Schrödinger model, SINDy.

Contents

1	Introduction	2
2	Model description	3
2.1	Dark soliton	4
2.2	Bright soliton	4
2.3	Multi-soliton construction	5
3	Data-driven methods	5
3.1	Sparse identification of nonlinear dynamics	6
3.2	SINDy with controls	7

^{*}Email: suyang@umass.edu

4 Numerical results	7
4.1 Data generation	7
4.2 Interaction of dark solitons	8
4.2.1 Two dark solitons without parabolic trap potential	8
4.2.2 Four dark solitons without parabolic trap potential (no interaction across boundary)	9
4.2.3 Four dark solitons without parabolic trap potential (with interaction across boundary)	9
4.2.4 One dark soliton with parabolic trap potential	10
4.2.5 Two dark solitons with parabolic trap potential	10
4.2.6 Four dark solitons with parabolic trap potential	11
4.3 Interaction of bright solitons	12
4.3.1 One bright soliton with parabolic trap	13
4.3.2 Two bright solitons without parabolic trap	13
4.3.3 Two bright solitons with parabolic trap	14
4.3.4 Multiple degrees of freedom: A case example	14
5 Conclusions and future directions	15

1 Introduction

Solitary waves [1, 2, 3, 4] constitute ubiquitous nonlinear structures in numerous mathematical physics and biology models, when the interplay of dispersion and nonlinearity is at hand. Some well-known models such as the Korteweg–De Vries (KdV) equation and nonlinear Schrödinger equation (NLS) serve as prototypical partial differential equations of the dispersive nonlinear type for modeling solitary-wave interactions. Indeed, their generic emergence from other models, through multiple scale expansions [5], renders them practically “normal form” type scenarios for associated dynamics.

In recent years, there has been a growing interest within the nonlinear-wave community towards studying the interactions between multiple solitons [6, 7, 8]; indeed the relevant topic has been also extensively addressed in both reviews [9], as well as books [10]. Notably, the emerging concept of *soliton gas* has been rigorously defined in the context of integrable systems as the asymptotic limit of the N -soliton solution [6]. It has been demonstrated that soliton interactions within a soliton gas can be effectively studied through both numerical and quasi-analytical approaches [11, 12, 13, 14, 15]. In such settings, a large cohort of solitary waves dynamically evolves through a dense array of interaction events.

A complementary, time-honored approach over many decades [16, 17, 18, 19, 9, 20, 7] has been to try to characterize the dynamics of few (typically two, and building from there) solitary waves, extending then considerations to larger clusters of structures; see, e.g., [8]. It is important to appreciate that such low-dimensional descriptions have been of particular value not only in the context of one-dimensional structures such as solitary waves, but also in higher-dimensional settings, as in the realm of vortices [21, 22, 23], or vortex rings [24, 25]. Accordingly, direct numerical simulations have been extensively complemented by (and compared to) reduced-order modeling of soliton (as well as vortex etc.) interactions. Such a reduction of the original partial differential equation (PDE) dynamics to the (here referred to as) “soliton manifold” plays an important role in understanding the underlying dynamics and has been used for building “superstructures”, including hypersolitons [solitons on lattices built out of soliton interactions] [7], vortex crystals [stationary patterns of many vortices [21, 22]] etc. This approach involves approximating the evolution of key soliton characteristics via a system of ordinary differential equations (ODEs), a feature that may not just be theoretically attainable, but also experimentally probed, e.g., for bright [26], as well as for dark [27] solitary structures.

So far, for the nontrivial task of deriving such effective “particle like” descriptions, we have been heavily relying on physical expert approaches. These involve a variety of techniques, including notably ones that are based on the variational structure of the problem and the selection of a suitable ansatz [9] (see also [10] for a recent discussion). Here the ansatz incorporates some of the key features of the wave, such as its amplitude, width, center position and velocity, among others, and a substitution of the ansatz in the model’s

Lagrangian or Hamiltonian enables the usage of Euler-Lagrange or Hamilton type equations for the effective time-dependent parameters. This represents effectively a “projection” (rigidly selected by an expert) of the partial differential equation (PDE) dynamics on the soliton manifold. While this appears restricted to Hamiltonian systems, extensions do systematically exist for open dynamical settings, such as, e.g., through the work of [28]. On the other hand, there exist similar techniques that are based on asymptotic projection methods at the level of the original partial differential equations [29, 23] (e.g., in the context of vortices) that also yield similar results. Similar results are also obtained based on soliton perturbation theory [17]. In all of these classes of methods, expert ansatz selection and detailed mathematical (variational, asymptotic or perturbative) analysis is leveraged to obtain the effective ODEs for the wave interactions.

Here, we would like to advocate an alternative, complementary, data-driven perspective toward this problem of obtaining a suitable dynamical projection to the “soliton manifold” and the resulting ODEs. Indeed, discovering governing equations has become a central theme in the field of dynamical systems. Various numerical algorithms and machine learning methods [30, 31, 32, 33, 34] have been proposed for this purpose and all of them have proven to be valuable, under suitable circumstances. In this work, we focus on the methodology referred to as Sparse Identification of Nonlinear Dynamics (SINDy) [30], a sparse regression-based algorithmic framework designed to identify parsimonious dynamical models from time series data. Specifically, as a prototypical benchmark problem of its kind, we apply SINDy to discover reduced ODE models governing soliton interactions in the nonlinear Schrödinger system. In addition to the standard SINDy formulation, we also explore the use of its extension, SINDy with control [35], which incorporates external inputs or known constraints during the identification process. Our intention is to illustrate both the potential successes, but also the possible problems that such a mainstream data-driven algorithmic platform may encounter in performing fundamental soliton manifold projections/deriving solitonic ODE dynamics. In so doing, we hope to elucidate both some of the technical steps needed to bring the methodology to the realm of applicability, the comparison with some well-benchmarked theoretical results and to highlight some of the improvements that will be needed in order to further such a data-driven methodology to the realm of problems that are considerably more complex/not easily accessible theoretically.

The outline of this paper is arranged as follows. In section 2, we provide a detailed description of the model which is considered in this work. In addition, we review some well-known analytical soliton solutions (both dark and bright solitons), and we also discuss some reduced dynamical systems which some particular features of the solitons satisfy. Finally, we also construct the multi-soliton initial data which shall be utilized in our numerical experiments. Next, in section 3, we briefly review (for completeness) the SINDy algorithm which is the central methodological tool used for the data-driven derivation of solitonic ODEs within this work. In section 4, we showcase the numerical results obtained in connection to the dynamical systems identification by applying SINDy. Here, we highlight both the cases where SINDy works quite well (in comparison to the well-known benchmark cases), but also the ones where it doesn’t and endeavor to rationalize such less successful outcomes and when the interested practitioners may expect ones such. Finally, Section 5 concludes the paper with a summary of findings and suggestions for a number of emerging research directions in this theme at the nexus of data science and nonlinear waves that we believe merits further study.

2 Model description

The model we will consider in this paper is the one-dimensional Gross-Pitaevskii (GP) equation, which serves as a variant of the standard NLS equation with an external potential. This is the canonical mean-field model for ultracold atoms in the presence of external confinement [36, 37], although it is also of relevance in nonlinear optics in the presence of spatially varying refractive index [9]. Specifically, we study the following equation:

$$iu_t = -\frac{1}{2}u_{xx} + g|u|^2u + V_{\text{MT}}(x)u, \quad (2.1)$$

where $g = \pm 1$ determines the focusing ($g = -1$) or defocusing ($g = +1$) nonlinearity, and $V_{\text{MT}}(x) = \frac{1}{2}\Omega^2 x^2$ refers to a harmonic (magnetic) trapping potential with a real constant Ω . Unless otherwise specified, we fix $\Omega = 0.025$ [motivated by the feature that Ω represents a ratio of longitudinal to transverse confinement and for the relevant reduction to be valid needs to be $\Omega \ll 1$] in all numerical experiments presented in this paper.

2.1 Dark soliton

When $g = 1$ and in the absence of the trap, i.e., for $V_{\text{MT}} = 0$, it is well-known [20] that the model (2.1) admits the following exact dark soliton (DS) solution:

$$u_{\text{ds}}(x, t) = \sqrt{n_0} [B \tanh\{\sqrt{n_0}B[x - \xi(t)]\} + iA] e^{i\phi_{\text{ds}}(t)}, \quad (2.2)$$

where $n_0 \in \mathbb{R}^+$ is the density of the constant background supporting the dark soliton, and $\xi(t) = vt + \xi_0$ denotes the soliton position (with ξ_0 the initial location and v the velocity). The associated phase is

$$\phi_{\text{ds}}(t) = -n_0 t + \phi_0, \quad (2.3)$$

with ϕ_0 being the initial phase. The parameters A and B , together with the soliton velocity v , satisfy the relations $A^2 + B^2 = 1$ and $v = A\sqrt{n_0}$.

Assume there exist $N_s \in \mathbb{Z}^+$ dark solitons in a multi-dark-soliton state, then it is known that the dynamics of their positions approximately obey the following second-order ODE [18, 20, 7]:

$$\ddot{\xi}_i = 8n_0^{3/2}e^{2\sqrt{n_0}(\xi_{i-1}-\xi_i)} - 8n_0^{3/2}e^{2\sqrt{n_0}(\xi_i-\xi_{i+1})} - \omega^2\xi_i, \quad (2.4)$$

where $\omega = \Omega/\sqrt{2}$, ξ_i denotes the position of the i -th dark soliton in the chain, and $\ddot{\xi}_i = \frac{d^2}{dt^2}\xi_i$.

2.2 Bright soliton

On the other hand, when $g = -1$ and in the absence of the external potential (i.e., $V_{\text{MT}} = 0$), the one-dimensional GP equation (2.1) admits the following bright soliton (BS) solution [7],

$$u_{\text{bs}}(x, t) = a \operatorname{sech} \left[a(x - \xi(t)) \right] \exp \left[i(vx + \phi_{\text{bs}}(t)) \right], \quad (2.5)$$

where a is the amplitude of the bright soliton, $\xi(t) = \xi_0 + vt$ denotes the position, and $\phi_{\text{bs}} = \phi_0 + \frac{(a^2 - v^2)t}{2}$ is the associated phase. Here, ξ_0 and ϕ_0 represent the initial position and phase of the bright soliton, respectively.

Moreover, consider a chain of bright solitons, where the parameters of the i -th soliton are described by the vector $P_i = (a_i, \xi_i, v_i, \phi_i)$, where the four parameters represent the amplitude, position, velocity, and phase of the i -th soliton, respectively. It has been shown that the dynamical evolution of these parameters ought to be approximately described by the following system of first-order ODEs:

$$\begin{aligned} \dot{a}_j &= 4a_j^2(S_{j,j-1} - S_{j,j+1}), \\ \dot{v}_j &= -4a_j^2(C_{j,j-1} - C_{j,j+1}), \\ \dot{\xi}_j &= v_j - 2(S_{j,j-1} + S_{j,j+1}), \\ \dot{\phi}_j &= \frac{a_j^2 + v_j^2}{2} - 2v_j(S_{j,j-1} + S_{j,j+1}) + 6a_j(C_{j,j-1} + C_{j,j+1}), \end{aligned} \quad (2.6)$$

where

$$\begin{aligned} S_{j,n} &= \exp \left[-|a_n(\xi_j - \xi_n)| \right] a_n \sin(s_{j,n}\phi_{j,n}), \\ C_{j,n} &= \exp \left[-|a_n(\xi_j - \xi_n)| \right] a_n \cos(\phi_{j,n}), \\ \phi_{j,n} &= \phi_j - \phi_n - v_n(\xi_j - \xi_n), \\ s_{j,j-1} &= -s_{j,j+1} = 1; \end{aligned} \quad (2.7)$$

see for further details [7], as well as references therein. However, it is important to note that the system (2.6) is valid only under the following conditions: (i) all bright solitons considered need to have similar amplitudes and velocities. Mathematically, this requires that $|a_i - a_j| \ll \bar{a}$ and $|v_i - v_j| \ll \bar{v}$, where \bar{a}, \bar{v} denote the average amplitude and velocity of the bright solitons. (ii) All adjacent bright solitons need to be sufficiently well separated; this means that $\bar{a}|\xi_i - \xi_j| \gg 1$. (iii) All bright solitons need to satisfy the height-separation constraint: $|a_i - a_j||\xi_i - \xi_j| \ll 1$.

Moreover, when the three conditions (i)–(iii) are fulfilled, the system of ODEs in (2.6) can be, to a further degree of approximation (essentially rendering all a_i 's equal), reduced to the following second-order ODE,

$$\ddot{\xi}_i = \sigma_{i-1,i} 4a^3 \exp(-a(\xi_i - \xi_{i-1})) - \sigma_{i,i+1} 4a^3 \exp(-a(\xi_{i+1} - \xi_i)), \quad (2.8)$$

where $\sigma_{i,j} = \pm 1$ is determined by the relative phase of the two consecutive bright solitons. Specifically, when the solitons are out of phase (OOP), i.e., $|\phi_i - \phi_j| = \pi$, we have $\sigma_{i,j} = 1$, while $\sigma_{i,j} = -1$ when the solitons are in phase (IP), i.e., $\phi_i = \phi_j$. Moreover, for OOP bright solitons, when there exists a trap (i.e. $\Omega \neq 0$), the reduced dynamics of soliton interaction reads,

$$\ddot{\xi}_i = 4a^3 \exp(a(\xi_{i-1} - \xi_i)) - 4a^3 \exp(a(\xi_i - \xi_{i+1})) - \Omega^2 \xi_i; \quad (2.9)$$

i.e., the trap adds a longitudinal harmonic confinement of frequency Ω to each of the solitary waves [7].

2.3 Multi-soliton construction

To study the interaction dynamics of the bright or dark solitons in the GP equation (2.1), it is essential to construct appropriate initial data which we call the multi-soliton initial conditions. The procedures for generating these initial conditions differ between the bright and dark soliton cases.

For a chain of N dark solitons, the initial condition for the i -th dark soliton $u_{\text{ds}}^{(i)}$ leverages Eq. (2.2). Specifically, we define the initial state of N dark solitons through a product ansatz as:

$$u_{\text{ds}}(x, 0) = \prod_{i=1}^N u_{\text{ds}}^{(i)}(x, 0). \quad (2.10)$$

On the other hand, for the bright soliton case, we focus exclusively on OOP bright solitons, where the phases difference between adjacent solitons is π . In this scenario, the initial state of the bright soliton chain is constructed by summing the individual bright soliton profiles defined in Eq. (2.5). Namely, in this work, we utilize the following initial state for the bright soliton chain

$$u_{\text{bs}}(x, 0) = \sum_{i=1}^N (-1)^{i-1} \operatorname{sech}(x - \xi_i), \quad (2.11)$$

where each soliton is assumed to have constant unit amplitudes with zero velocities so as to fulfill the conditions (I), (II), and (III) described in sub-section 2.2.

3 Data-driven methods

In this section, we briefly review the data-driven method known as Sparse Identification of Nonlinear Dynamics (SINDy) [30], which serves as the primary framework for identifying soliton-interaction dynamics in the present setting. In addition to the standard SINDy approach, we also discuss an extended variant, SINDy with control [35], which is likewise a relevant methodology for our study. Essentially, what this method achieves is that users have the flexibility to choose their customized time-series dataset (augmenting the ones of the state variables) which can be directly added to the library, and these customized time-series data are the so-called control inputs.

3.1 Sparse identification of nonlinear dynamics

SINDy [30] is a powerful data-driven method whose scope is to discover governing ODEs (or PDEs, where appropriate) based on simulated or observational data and the selection of suitable user-selected/supplied libraries. Mathematically, we consider the following dynamical system

$$\frac{dx}{dt} = f(x), \quad (3.1)$$

where $x(t) = (x_1(t), x_2(t), \dots, x_n(t)) \in \mathbb{R}^n$ is the state variable at the particular time t , and $f: \mathbb{R}^n \rightarrow \mathbb{R}^n$ refers to a nonlinear mapping which governs the evolution dynamics of the state x . The goal of SINDy is to identify an approximate representation of the (unknown) governing function f given a time series of state observations $x(t)$.

The fundamental assumption of SINDy is that the nonlinear mapping f has a “simple” expression, allowing it to be approximated as a linear combination of a small number of terms from a prescribed library, denoted as $\theta(x) = [\theta_1(x), \theta_2(x), \dots, \theta_p(x)]$, where each $\theta_j(x), j \in [1, 2, \dots, n]$ is a nonlinear candidate feature function. Typical choices for $\theta_j(x)$ include sinusoidal, polynomials, exponentials, and other nonlinearities commonly encountered in physical models. The user can also supply relevant terms, based on physical expertise when that is available for the system in question.

In particular, SINDy assumes the right-hand side nonlinear dynamics of Eq. (3.1) can be approximated in the following way

$$f(x) = [f_1(x), f_2(x), \dots, f_n(x)] \approx \theta(x) \cdot \Xi = [\theta_1(x), \theta_2(x), \dots, \theta_p(x)] \cdot [\xi_1, \xi_2, \dots, \xi_n], \quad (3.2)$$

where $\Xi = [\xi_1, \xi_2, \dots, \xi_n] \in \mathbb{R}^{p \times n}$ is a sparse matrix. Each column $\xi_i \in \mathbb{R}^p$ determines which terms from the library $\theta(x)$ are selected to represent the component function $f_i(x)$ of the dynamics.

To identify the sparse coefficient matrix Ξ , SINDy performs sparse regression on the data. Specifically, we consider the time-series data of the state $x(t)$, given by $[x(t_1), x(t_2), \dots, x(t_N)] \in \mathbb{R}^{n \times N}$ at discrete time snapshots of t_1, t_2, \dots, t_N . Then we have the following data matrix and corresponding time-derivative matrix:

$$X = [x(t_1), x(t_2), \dots, x(t_N)]^T = [X_1, X_2, \dots, X_n] = \begin{bmatrix} x_1(t_1) & x_2(t_1) & \dots & x_n(t_1) \\ x_1(t_2) & x_2(t_2) & \dots & x_n(t_2) \\ \vdots & \vdots & \ddots & \vdots \\ x_1(t_N) & x_2(t_N) & \dots & x_n(t_N) \end{bmatrix} \in \mathbb{R}^{N \times n},$$

$$\frac{dX}{dt} = [\dot{x}_1(t_1), \dot{x}_2(t_1), \dots, \dot{x}_n(t_1)] = \begin{bmatrix} \dot{x}_1(t_1) & \dot{x}_2(t_1) & \dots & \dot{x}_n(t_1) \\ \dot{x}_1(t_2) & \dot{x}_2(t_2) & \dots & \dot{x}_n(t_2) \\ \vdots & \vdots & \ddots & \vdots \\ \dot{x}_1(t_N) & \dot{x}_2(t_N) & \dots & \dot{x}_n(t_N) \end{bmatrix} \in \mathbb{R}^{N \times n}, \quad (3.3)$$

where the derivative matrix $\frac{dX}{dt}$ can, for example, be numerically approximated from the data matrix X using a finite-difference scheme [naturally, any derivative approximation method will involve a certain error, with the numerical method aiming to minimize such error]. We then define the library matrix $\Theta(X) \in \mathbb{R}^{N \times p}$ as follows

$$\Theta(X) = [\theta_1(X), \theta_2(X), \dots, \theta_p(X)]. \quad (3.4)$$

Combining Eq. (3.1) and (3.2) yields the following problem

$$\frac{dX}{dt} \approx \Theta(X) \Xi, \quad (3.5)$$

To compute the sparse matrix Ξ , one may employ various techniques such as LASSO-type sparse regression, sequentially thresholded least-square regression [38] (STLSQ), or forward regression orthogonal least-squares [39] (FROLS). In this work, we primarily adopt STLSQ and FROLS as the main optimization strategies for identifying the governing equations of soliton-interaction dynamics.

It is worth noting that the optimizer FROLS is a greedy algorithm that incrementally selects terms based on their correlation with the residual. In all our numerical experiments involving FROLS, we limit the maximum number of iterations to two. This choice is motivated by the observation that, based on the approximated dynamics of the interactions of both bright and dark solitons, only a few terms are involved in the right-hand side of the ODEs. Therefore, we select only the most relevant terms that exhibit the strongest correlation with the input time series data, ensuring both model sparsity and interpretability.

3.2 SINDy with controls

SINDy with controls [35] extends the standard SINDy framework described in Subsection 3.1. In particular, we consider the following nonlinear dynamical system:

$$\frac{dx}{dt} = f(x, u), \quad (3.6)$$

where the u variable denotes the input control.

Given the time-series data of both the state x and the control u , Eq. (3.5) becomes

$$\frac{dX}{dt} \approx \Theta(X, U)\Xi, \quad (3.7)$$

where $U = [u_1, u_2, \dots, u_n]^T$ is the data set of the controls.

As in the standard case, performing sparse regression on Eq. (3.7) yields the solution for the sparse matrix Ξ that describes the dynamics.

4 Numerical results

In this section, we present numerical results on identifying soliton-interaction dynamics using both the standard SINDy method and its control-augmented variant. We divide this section into three subsections: Subsection 4.1 provides some preliminaries on how our dataset are processed and generated. Subsection 4.2 focuses on the data-driven discovery of interaction dynamics for dark solitons, while Subsection 4.3 presents the corresponding results for bright solitons.

4.1 Data generation

Before we display our numerical results on the identification of soliton interaction dynamics, it is important to first understand how our dataset is generated. Firstly, we note that we apply the RK4 time integration scheme with a finite-difference discretization of space to numerically solve Eq. (2.1). On the one hand, for the generation of the data for the positions of both bright and dark solitons, we first numerically pinpoint the x coordinates of all the global peaks (maxima or minima, respectively) of the intensity of the wave function (i.e. $|u(x, t)|^2$) and we shall treat the values of these x coordinates as the rough estimates of the locations of the solitons. Notice that we repeat such a process for every time snapshot t so as to obtain the time-series data that we denote as $\tilde{\xi}(t)$. However, it is not appropriate to directly use $\tilde{\xi}(t)$ since it is only a rough estimate of the soliton positions and the smoothness of such a dataset is suboptimal. Based on $\tilde{\xi}(t)$, we then perform a least-square fitting on the profile of the solitons, centered at $\tilde{\xi}(t)$, to further enhance the smoothness of the time-series data of soliton positions. Finally, we obtain our dataset for the position of the solitons, which is denoted as $\xi(t)$ in this paper. On the other hand, the data for the velocity $v(t)$ of the solitons are simply obtained by performing finite difference on the position time-series data of $\xi(t)$. Thirdly, the data for amplitudes, denoted as $a(t)$, of the (bright) solitons are obtained by numerically computing the maximum of the absolute value of the wave function (i.e. $|u(x, t)|$). Finally, for the phase time-series data $\phi(t)$ of the solitons, we calculate and treat the phase angles of the wave function $u(x, t)$ centered at $\xi(t)$ as our data for $\phi(t)$.

4.2 Interaction of dark solitons

We begin by investigating the interaction dynamics of dark solitons using the standard SINDy framework. In particular, we examine cases involving two and four interacting dark solitons [such cases with even soliton numbers are conducive to the use of periodic boundary conditions]. Here, we aim to identify the governing equations for their respective positions. Beyond varying the number of solitons in the chain, we also examine the effect of an external parabolic trap potential, with the goal of capturing how this additional influence modifies the underlying dynamics and contributes to the identification of accurate reduced-order models for dark soliton interactions.

4.2.1 Two dark solitons without parabolic trap potential

We start our investigation by examining the situation where only two dark solitons interact. For simplicity, we fix the background density to $n_0 = 1$, although our results can straightforwardly be extended to other values of n_0 . The dynamics governed by Eq. (2.1) are simulated using a fourth-order Runge–Kutta method for time integration and a finite-difference scheme for spatial discretization, under periodic boundary conditions. This simulation generates the time-series data required as input for the SINDy algorithm. Also note that SINDy is only applicable for a first-order ODE system, so we rewrite Eq. (2.4) as

$$\begin{aligned}\dot{\xi}_i &= v_i, \\ \dot{v}_i &= 8n_0^{3/2} e^{2\sqrt{n_0}(\xi_{i-1}-\xi_i)} - 8n_0^{3/2} e^{2\sqrt{n_0}(\xi_i-\xi_{i+1})}.\end{aligned}\quad (4.1)$$

where the term $-\omega^2 \xi_i$ is missing due to the absence of the parabolic trap potential. Then, our input time-series data, denoted by \mathbf{X} , are

$$\mathbf{X} = [\xi_1, \xi_2, \dot{\xi}_1, \dot{\xi}_2] = [\xi_1, \xi_2, v_1, v_2], \quad (4.2)$$

where the two first-order derivatives of $\dot{\xi}_1, \dot{\xi}_2$ are computed numerically by the central difference scheme.

We numerically solve the Eq. (2.1) with the initial condition (2.4) but with three distinct sets of initial positions and velocities. The resulting time-series data, denoted by $\mathbf{X}_1, \mathbf{X}_2, \mathbf{X}_3$, are then concatenated vertically as:

$$\mathbf{X} = \begin{bmatrix} \mathbf{X}_1 \\ \mathbf{X}_2 \\ \mathbf{X}_3 \end{bmatrix}. \quad (4.3)$$

Motivated by the structure of the approximate dynamical equations in Eq. (4.1), we define the SINDy library to include the following three candidate terms: $\Theta = [x, x^2, \exp(2(x - y))]$, where x, y refer to the terms in the set of the time-series data: $[\xi_1, \xi_2, v_1, v_2]$. As a result, there are totally $8 + \binom{4}{2} = 14$ terms in the library. With the input time-series data (4.3), the SINDy prediction reads,

$$\begin{aligned}\dot{\xi}_1 &= 1.000 v_1, \\ \dot{\xi}_2 &= 1.000 v_2, \\ \dot{v}_1 &= -7.990 \exp(2(\xi_1 - \xi_2)), \\ \dot{v}_2 &= 7.988 \exp(2(\xi_1 - \xi_2)).\end{aligned}\quad (4.4)$$

In this scenario, we notice that the SINDy prediction (4.4) accurately recovers the approximate dynamics of the dark-soliton interactions described in Eq. (4.1). This is further illustrated in the left panel of Figure 1, where the evolution of the two dark solitons predicted by SINDy closely aligns with the analytically derived system (2.4). Crucially, such a result requires the use of concatenated time-series data generated from multiple distinct initial conditions. When SINDy is applied using data from only a single initial condition, the resulting model fails to capture the correct dynamics due to overfitting and deviates substantially from the accurate prediction in Eq. (4.4).

4.2.2 Four dark solitons without parabolic trap potential (no interaction across boundary)

We now turn to the SINDy prediction for the interaction dynamics of four dark solitons. In this case, we do not account for the interaction between the first and last soliton, as the total simulation time is chosen to ensure that these solitons remain well separated from the domain boundaries and thus interact only negligibly. Indeed, in the current setting the outer soliton interaction is screened by the presence of the intermediate solitons and hence is exponentially weaker than the dominant terms of interest.

Before applying SINDy for dynamical prediction, we sample time-series data from two distinct initial conditions and concatenate them in a manner similar to Subsection 4.2.1. Here, we notice that the library includes: $\Theta = \{x, \exp(2(x - y))\}$, where $x, y \in [\xi_1, \xi_2, \xi_3, \xi_4, v_1, v_2, v_3, v_4]$, so in total there are $8 + \binom{8}{2} = 36$ terms. The resulting SINDy prediction is then given by:

$$\begin{aligned} \dot{\xi}_1 &= 1.000v_1, \\ \dot{\xi}_2 &= 1.000v_2, \\ \dot{\xi}_3 &= 1.000v_3, \\ \dot{\xi}_4 &= 1.000v_4, \\ \dot{v}_1 &= -8.016 \exp(2(\xi_1 - \xi_2)), \\ \dot{v}_2 &= 8.021 \exp(2(\xi_1 - \xi_2)) - 8.010 \exp(2(\xi_2 - \xi_3)), \\ \dot{v}_3 &= 8.011 \exp(2(\xi_2 - \xi_3)) - 8.007 \exp(2(\xi_3 - \xi_4)), \\ \dot{v}_4 &= 8.018 \exp(2(\xi_3 - \xi_4)). \end{aligned} \tag{4.5}$$

Similarly, SINDy successfully recovers the analytically approximated dark-soliton interaction dynamics described in system (2.4), with the right panel of Figure 1 providing further evidence for the close agreement between the analytically derived trajectories and those predicted by SINDy. It is perhaps worthwhile to note in passing that both in this example and the previous one, while the results were highly accurate as concerns the prediction of interactions and well in line with theoretical expectations from earlier works such as as [18, 27, 40], they did seem to involve slightly unequal coefficients, which is slightly “misaligned” with Newton’s third (equal action-reaction) law. We will return to address that point in subsequent sections.

4.2.3 Four dark solitons without parabolic trap potential (with interaction across boundary)

To explore the influence of boundary-induced interactions, we consider a longer simulation time that allows the first and last solitons to reach opposite boundaries and interact. To be more specific, we simulate the GP equation (2.1) with a sufficiently large total simulation time so that both of these two dark solitons can travel to the boundaries of the computational domain so that they can interact. The corresponding SINDy-identified model is:

$$\begin{aligned} \ddot{\xi}_1 &= -7.994 \exp(2(\xi_1 - \xi_2)) + 8.007 \exp(-2|2L - |\xi_1 - \xi_4||), \\ \ddot{\xi}_2 &= 8.002 \exp(2(\xi_1 - \xi_2)) - 7.994 \exp(2(\xi_2 - \xi_3)), \\ \ddot{\xi}_3 &= 8.001 \exp(2(\xi_2 - \xi_3)) - 8.001 \exp(2(\xi_3 - \xi_4)), \\ \ddot{\xi}_4 &= 8.005 \exp(2(\xi_3 - \xi_4)) - 8.001 \exp(-2|2L - |\xi_1 - \xi_4||), \end{aligned} \tag{4.6}$$

where $L = 30$ denotes one half of the length of the computational domain. We notice that the second term on the right-hand side of $\ddot{\xi}_1$ and $\ddot{\xi}_4$ in system (4.6) represents the interaction between the first and the last dark soliton. Notice that the library used in this example is: $\Theta = \{x, x^2, \exp(2(x - y)), \exp(-2|2L - |x - y||)\}$, i.e., it also involves the interaction term induced due to the presence of the “periodic boundary”, that is it takes into account the fact that the simulation occurs on a ring. Notice that the SINDy with control method is applied to this example, where the control inputs include $\xi_1, \xi_2, \xi_3, \xi_4$, and the original input time-series are $\dot{\xi}_1, \dot{\xi}_2, \dot{\xi}_3, \dot{\xi}_4$ so this means there are $2 \times 8 + 2 \times \binom{8}{2} = 72$ terms in the library.

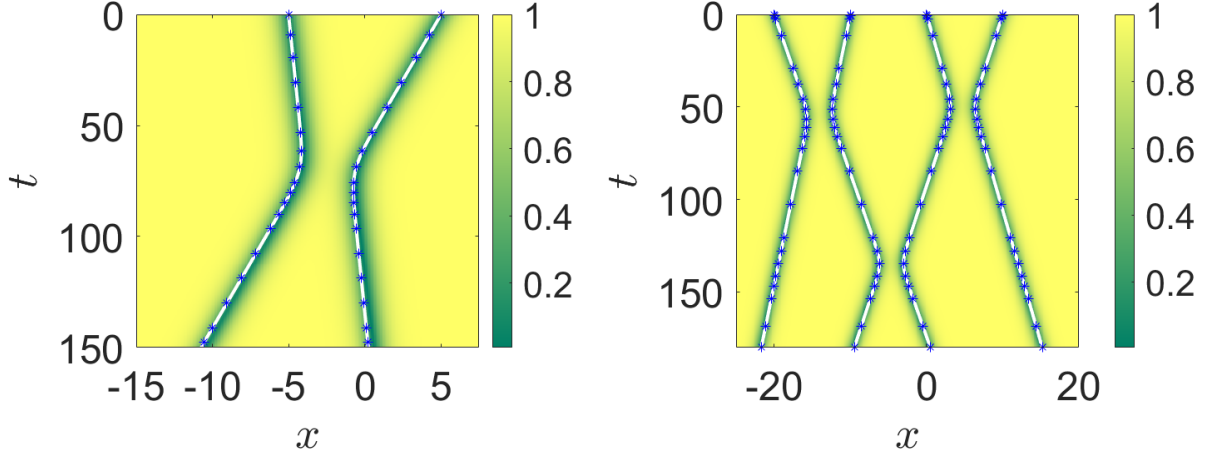


Figure 1: The spatio-temporal plot of dark-soliton interaction dynamics without a parabolic trap potential: the left panel shows the interaction of two dark solitons, while the right panel presents that of four dark solitons. Notice that the white solid curves and blue asterisks refer to theoretical prediction of the soliton positions based on system (2.4) and on the SINDy prediction based on (4.4) (two dark solitons) and (4.5) (four dark solitons), respectively.

4.2.4 One dark soliton with parabolic trap potential

Next, we examine the case where a parabolic trap potential is incorporated into the GP equation (2.1). In particular, we set the potential to $V_{MT} = \frac{1}{2}\Omega^2 x^2$ with $\Omega = 0.025$. We first investigate the position dynamics ξ of a single dark soliton. The SINDy with control is applied in this example: the control variable is ξ , while the input data is $\dot{\xi}$. The library is $\Theta = \{\exp(2(x - y)), x, x^2\}$, so there are totally $2 \times 2 + \binom{2}{2} = 5$ terms. Here, the SINDy prediction yields:

$$\ddot{\xi} = -0.00031287\xi. \quad (4.7)$$

We first notice that the dynamics (4.7) is learned by applying the SINDy with control via the FROLS optimizer, which is a greedy method. Motivated by the structure of the approximate dynamics in Eq.(2.4), we focus on selecting a single dominant term on the right-hand side that governs the evolution of the dark soliton's position.

Furthermore, we construct a library: $\Theta = \{\exp(2(x - y)), x, x^2, \dots, x^{10}\}$, where $x, y \in \{\dot{\xi}, \xi\}$. We notice that it is not physically meaningful to have interaction between the two terms of ξ and $\dot{\xi}$ as these two quantities even have different units. Nevertheless, SINDy chooses to ignore relevant interactions between these two terms, and its prediction is still reasonable. In summary, the SINDy model consistently and robustly recovers the expected single-soliton dynamics, accurately reflecting the analytical structure given of the reduced single-soliton ODE.

4.2.5 Two dark solitons with parabolic trap potential

In the process of sampling the time-series data used for SINDy implementation, we take $\Omega = 0.025$. We then apply the method of SINDy with control. Here, the library is $\Theta = \{x, x^2, \exp(2(x - y))\}$. The input time-series data are $[\dot{\xi}_1, \dot{\xi}_2]$, while the control variables are $[\xi_1, \xi_2]$. Hence, there are totally $2 \times 4 + \binom{4}{2} = 14$ terms. The resulting dynamics, as predicted by SINDy reads:

$$\begin{aligned} \ddot{\xi}_1 &= -7.757 \exp(2(\xi_1 - \xi_2)) - 0.00031635\xi_1, \\ \ddot{\xi}_2 &= 7.803 \exp(2(\xi_1 - \xi_2)) - 0.00031674\xi_2. \end{aligned} \quad (4.8)$$

It is evident that the SINDy prediction in Eq.(4.8) closely aligns with the approximated dynamics described by Eq.(2.4).

Nevertheless, it should be highlighted that now the deviations are more pronounced. This is due to two different features. On the one hand, the Newton's third law "imbalance" between the interaction terms is somewhat more pronounced. On the other hand, here the interactions are screened by the presence of the density modulation; similar examples have appeared in the literature also in the context of vortices when the density is inhomogeneous, with a relevant example being, e.g., the work of [41]. This may be partially reflected in the interaction coefficient deviation from the homogeneous expectation of the prefactor of 8 [18].

4.2.6 Four dark solitons with parabolic trap potential

We then test and extend the result of Eq. (4.8) to the case of a chain where four dark solitons are involved. Here too, we utilize a library involving $\Theta = \{x, x^2, \exp(2(x - y))\}$. The input data are $\dot{\xi}_1, \dot{\xi}_2, \dot{\xi}_3, \dot{\xi}_4$, and the control variables are $\xi_1, \xi_2, \xi_3, \xi_4$, so there are totally $2 \times 8 + \binom{8}{2} = 44$ terms. Applying the method of SINDy with control again in this case, the predicted dynamics for the time-series $[\ddot{\xi}_1, \ddot{\xi}_2, \ddot{\xi}_3, \ddot{\xi}_4]$ reads,

$$\begin{aligned}\ddot{\xi}_1 &= -7.950 \exp(2(\xi_1 - \xi_2)) - 0.00031272 \xi_1, \\ \ddot{\xi}_2 &= 8.420 \exp(2(\xi_1 - \xi_2)) - 7.506 \exp(2(\xi_2 - \xi_3)), \\ \ddot{\xi}_3 &= 7.522 \exp(2(\xi_2 - \xi_3)) - 8.406 \exp(2(\xi_3 - \xi_4)), \\ \ddot{\xi}_4 &= 7.900 \exp(2(\xi_3 - \xi_4)) - 0.00031206 \xi_4.\end{aligned}\tag{4.9}$$

We observe that the SINDy-predicted dynamical equations for the dark-soliton positions are less accurate than expected. For instance, the model fails to capture the parabolic-trap contribution for the second and third solitons in the chain. Specifically, the terms $\frac{\Omega^2}{2} \dot{\xi}_2$ and $\frac{\Omega^2}{2} \dot{\xi}_3$ should appear on the right-hand sides of $\ddot{\xi}_2$ and $\ddot{\xi}_3$, respectively. Moreover, the recovered equation, once again, and in this case more manifestly, violates Newton's third law, as the interaction forces between solitons are not equal and opposite. It is interesting to observe at an interpretational level that the resulting regression example appears to trade off some of the interaction force with the effect of the parabolic confinement on solitons 2 and 3, and again to note the effect of the curvature of the wavefunction profile apparently leading to (in this case, more substantial) deviations from the homogeneous coefficient of 8 in the case of the pairwise forces.

For these reasons, we propose a simple, physics-informed alternative to identify a better and more consistent (also compliant with Newton's third law) set of dynamical equations for the four soliton positions, written in the following matrix form,

$$Y = X\beta, \tag{4.10}$$

where

$$\begin{aligned}Y &= [\ddot{\xi}_1, \ddot{\xi}_2, \ddot{\xi}_3, \ddot{\xi}_4], \\ X &= [\exp(2(\xi_1 - \xi_2)), \exp(2(\xi_2 - \xi_3)), \exp(2(\xi_3 - \xi_4)), \xi_1, \xi_2, \xi_3, \xi_4],\end{aligned}\tag{4.11}$$

and β denotes the following coefficient matrix with the unknown positive entries $a, b, c, d > 0$,

$$\beta = \begin{bmatrix} -a & a & 0 & 0 \\ 0 & -b & b & 0 \\ 0 & 0 & -c & c \\ -d & 0 & 0 & 0 \\ 0 & -d & 0 & 0 \\ 0 & 0 & -d & 0 \\ 0 & 0 & 0 & -d \end{bmatrix}. \tag{4.12}$$

Essentially, for this choice of β , we assume that the pairwise interactions between solitons obey Newton's third law. In what follows, we elucidate how Eq. (4.10) can be reformulated as a linear regression problem for the unknown variables $[a, b, c, d]$. Specifically, observe that the system (4.10) can be rewritten as

$$\tilde{Y} = \tilde{X}\tilde{\beta}, \tag{4.13}$$

where

$$\begin{aligned}\tilde{Y} &= \begin{bmatrix} \ddot{\xi}_1 \\ \ddot{\xi}_2 \\ \ddot{\xi}_3 \\ \ddot{\xi}_4 \end{bmatrix}, \\ \tilde{X} &= \begin{bmatrix} -\exp(2(\xi_1 - \xi_2)) & \vec{0}_{N \times 1} & \vec{0}_{N \times 1} & -\xi_1 \\ \exp(2(\xi_1 - \xi_2)) & -\exp(2(\xi_2 - \xi_3)) & \vec{0}_{N \times 1} & -\xi_2 \\ \vec{0}_{N \times 1} & \exp(2(\xi_2 - \xi_3)) & -\exp(2(\xi_3 - \xi_4)) & -\xi_3 \\ \vec{0}_{N \times 1} & \vec{0}_{N \times 1} & \exp(2(\xi_3 - \xi_4)) & -\xi_4 \end{bmatrix}, \\ \tilde{\beta} &= [a, b, c, d]^T,\end{aligned}\tag{4.14}$$

where $\vec{0}_{N \times 1}$ denotes the N by 1 zero column vector.

We observe that both the left- and right-hand sides of Eq.(4.13) are $4N \times 1$ column vectors, where N denotes the length of the time series of ξ_i . In addition, we note that Eq. (4.13) is a standard linear model, and the solution for $\tilde{\beta}$ reads, by solving the relevant least square optimization problem,

$$\tilde{\beta} = (\tilde{X}^T \tilde{X})^{-1} \tilde{X}^T \tilde{Y}.\tag{4.15}$$

Through the numerical implementation of (4.15), we have (keeping the final numeric results up to the third decimal point) that

$$\tilde{\beta} = [8.006, \quad 7.642, \quad 7.983, \quad 0.0003176]^T.\tag{4.16}$$

Finally, the physics-informed dynamical system of positions of the four dark solitary waves reads

$$\begin{aligned}\ddot{\xi}_1 &= -8.006 \exp(2(\xi_1 - \xi_2)) - 0.0003176 \xi_1, \\ \ddot{\xi}_2 &= 8.006 \exp(2(\xi_1 - \xi_2)) - 7.642 \exp(2(\xi_2 - \xi_3)) - 0.0003176 \xi_2, \\ \ddot{\xi}_3 &= 7.642 \exp(2(\xi_2 - \xi_3)) - 7.983 \exp(2(\xi_3 - \xi_4)) - 0.0003176 \xi_3, \\ \ddot{\xi}_4 &= 7.983 \exp(2(\xi_3 - \xi_4)) - 0.0003176 \xi_4.\end{aligned}\tag{4.17}$$

Admittedly, Eq. (4.17) does not perfectly match the theoretically derived reduced-order model for the four-soliton interaction dynamics under a harmonic trap. However, as per the screening effect of the inhomogeneous density discussed above (see also [41]), this level of deviation may be reasonable to expect. This system already provides a significantly improved recovery of the dynamics compared to its physics-agnostic counterpart, Eq. (4.9). Such a claim can also be quantitatively verified by comparing the L^∞ loss of the time-series dataset of the soliton positions based on system (4.9) with that of dataset according to system (4.17). We first notice that the L^∞ loss of a given time-series data $\xi = (\xi_i)_{i=1}^N$ is defined as follows,

$$L_{\text{loss}}^\infty(\xi) = \max_{1 \leq i \leq N} \left(\left| \xi_i - \xi_i^{\text{GT}} \right| \right),\tag{4.18}$$

where ξ^{GT} refers to the ground-truth data sampled from the original PDE (2.1). The L^∞ loss is 0.478 for the the system of Eqs. (4.17) (incorporating the relevant physical principles/intuition), while it is an order of magnitude larger for the Physics-agnostic system of Eqs. (4.9). Moreover, Fig. (2) further demonstrates at the level of trajectories how the Physics-informed prediction (4.17) of the dark-soliton positions performs much better than the “standard” SINDy prediction (4.9).

4.3 Interaction of bright solitons

We now shift our focus to the interaction dynamics of bright solitons. For conciseness (and having illustrated some of the issues that arise when going to a larger number of waves in the dark soliton case), in what follows, we restrict our analysis to the case of up to two interacting bright solitons. Similarly to the scenario of the dark solitons, we also investigate how the presence of a parabolic trapping potential affects the interaction dynamics within the bright-soliton chain.

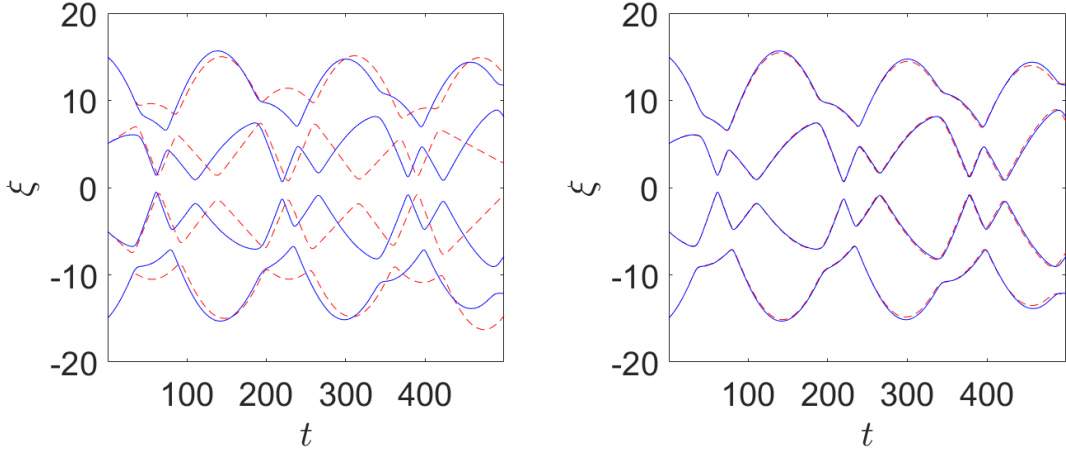


Figure 2: The comparisons of the SINDy predicted dark-soliton positions (based on Eq. (4.9)) and of the Physics-informed predicted dark-soliton positions (based on Eq. (4.17)) with that of ground-truth dark-soliton positions sampled from the PDE (2.1). Notice that the dashed red curves depict the SINDy and Physics-informed predicted trajectories of the dark-soliton positions, while the solid blue curve represents the ground-truth dark-soliton positions sampled from the PDE.

4.3.1 One bright soliton with parabolic trap

We first consider only a single bright soliton in the presence of a parabolic trap potential. In this case, the dynamical equation for the single bright soliton reads:

$$\ddot{\xi} = -\Omega^2 \xi. \quad (4.19)$$

The SINDy-identified model for the dynamics of a single bright soliton under the influence of a parabolic trapping potential (with $\Omega = 0.025$) is given by:

$$\ddot{\xi} = -0.00062491 \xi. \quad (4.20)$$

This result is obtained using an extended library that include power of ξ and of v up to order 10. The fact that SINDy selects only the linear term suggests that it robustly and accurately recovers the true underlying dynamics of the single bright soliton in this confined setting.

4.3.2 Two bright solitons without parabolic trap

Now, we examine the interaction dynamics of two bright solitons in the case where a parabolic trap is absent. we apply the method to time-series data generated from the following initial position of the two bright solitons:

$$\xi_0 = [-3, 3]. \quad (4.21)$$

Notice that the initial positions in system (4.21) mean that the first bright soliton is initially located at the position $x = -3$ while the second bright soliton at $x = 3$.

In these runs, the amplitude is $a = 1$ for both solitons. The library is: $\Theta = \{x, x^2, \exp(x - y), \exp(-|2L - |x - y||)\}$, where $x, y \in [\xi_1, \xi_2, \xi_1, \xi_2]$. The regular time-series input involves $\dot{\xi}_1, \dot{\xi}_2$, while the control variables (since we are once again using SINDy with control) are ξ_1, ξ_2 . The SINDy prediction in this case yields:

$$\begin{aligned} \ddot{\xi}_1 &= -4.539 \exp(\xi_1 - \xi_2) + 4.327 \exp(-|2L - |\xi_1 - \xi_2||), \\ \ddot{\xi}_2 &= 4.539 \exp(\xi_1 - \xi_2) - 4.327 \exp(-|2L - |\xi_1 - \xi_2||), \end{aligned} \quad (4.22)$$

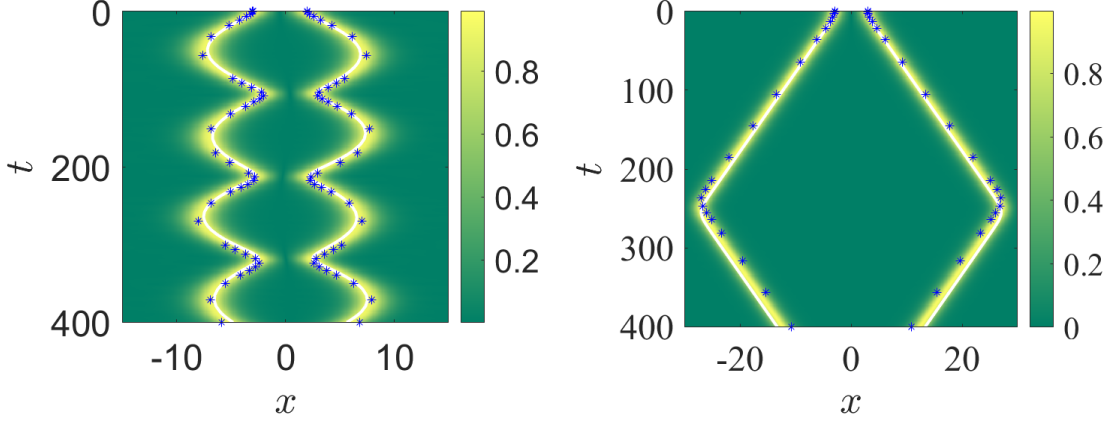


Figure 3: The spatio-temporal plot of the bright-soliton interaction in the presence of (Left panel) and without (Right panel) a parabolic trap potential. Notice that the solid white curves and the blue asterisks depict the theoretical prediction of the positions of the two bright solitons based on system (4.19) and the SINDy prediction on the soliton positions based on (4.23) and (4.22). The underlying contour map stems from the simulation of the original NLS PDE with the parabolic confinement.

Moreover, we have also tried another set of initial positions, which is $\xi_0 = [-2.5, 2.5]$, and the SINDy prediction yields a completely similar dynamics as the system (4.22).

Here, we find that the SINDy prediction in system (4.22) provides a reasonable approximation to the theoretically expected bright soliton interaction; for the latter the prefactor of Eq. (2.8) would have been equal to 4, while here we find it to be closer to 4.5. Nevertheless, the interaction accounting for the periodic nature of the domain is appropriately accounted for and a reasonably good fit to the dynamics is observed (See the right panel in Fig. 3 for such a comparison).

4.3.3 Two bright solitons with parabolic trap

We also investigate the interaction dynamics of two bright solitons in the presence of a parabolic trapping potential.

The SINDy-identified model for this scenario is given by:

$$\begin{aligned}\ddot{\xi}_1 &= -4.607 \exp(\xi_1 - \xi_2) - 0.000619 \xi_1, \\ \ddot{\xi}_2 &= 4.602 \exp(\xi_1 - \xi_2) - 0.000615 \xi_2.\end{aligned}\tag{4.23}$$

As one can see in Figure 3, when there is a harmonic trap, the SINDy prediction is reasonably accurate, matching well with the associated analytical approximated dynamics described in Eq. (2.9) and importantly with the underlying PDE contour map also depicted in the Figure.

4.3.4 Multiple degrees of freedom: A case example

Up to now, all previous numerical experiments have involved systems with only two degrees of freedom. Namely, the dynamics systems only consider the positions ξ and the velocities v of the solitons. To explore the capabilities of SINDy on higher-dimensional systems and also to illustrate some of the methodological limitations of the present approach, we now turn our attention to the full dynamical model with four degrees of freedom in the case of two bright solitons, as described by Eq. (2.6).

Similarly to what was discussed before, we generate all the necessary time-series data for all four relevant parameters of the bright solitons, namely the amplitude, position, velocity and phase thereof. Subsequently,

we examine SINDy's performance in this more complex setting. Due to the increased dimensionality, we restrict our investigation to the case of two interacting bright solitons, assuming they are out-of-phase, i.e., we have that $\sigma_{i,j} = 1$. Admittedly, this case is somewhat simpler to tackle than the one of the in-phase attractive interaction, especially so in the context of non-integrable models (where the solitons may exchange mass etc.). While these complications are worthwhile to consider in future work, we will steer clear of them here.

In the present case, the SINDy prediction for this four degrees-of-freedom dynamical system reads

$$\begin{aligned}\dot{a}_1 &= 0.841(-4a_1^2 S_{12}), & \dot{a}_2 &= 1.040(4a_2^2 S_{21}), \\ \dot{v}_1 &= 0.733(6a_2 C_{21}), & \dot{v}_2 &= -0.769(6a_2 C_{21}), \\ \dot{\xi}_1 &= 1.000v_1, & \dot{\xi}_2 &= 1.000v_2, \\ \dot{\phi}_1 &= 0.999\left(\frac{a_1^2 + v_1^2}{2}\right), & \dot{\phi}_2 &= 0.999\left(\frac{a_2^2 + v_2^2}{2}\right).\end{aligned}\tag{4.24}$$

Notice that in this case the library is $\Theta = \{x\}$ where

$$x \in \left[-4a_1^2 S_{12}, 4a_2^2 S_{21}, 4a_1^2 C_{12}, -4a_2^2 C_{21}, v_1, -2S_{12}, v_2, -2S_{21}, \frac{1}{2}(a_1^2 + v_1^2), -2v_1 S_{12}, 6a_1 C_{12}, \frac{1}{2}(a_2^2 + v_2^2), -2v_2 S_{21}, 6a_2 C_{21}\right].\tag{4.25}$$

All these terms are used as control variables in SINDy. Finally, for this multi-degree case example, the optimizer we used was the usual greedy algorithm FROLS.

It is worthwhile to note that unfortunately, in this more complex, multi-degree case example, SINDy fails to yield a prediction which closely aligns with the corresponding approximated dynamics listed in system (2.6). However, based on its prediction, as depicted in Figure 4, SINDy's predicted dynamics (in dashed-dotted blue) is still capable to qualitatively capture the evolution dynamics of the four distinct characteristics of the solitons (in solid black, as obtained from the PDE simulation). Moreover, it is also worthwhile to notice that in this particular example, the theoretical prediction based on system (2.6) also deviates from the actual dynamics. Indeed, one can argue that the SINDy results are comparably good, if not better than the ones obtained variationally.

On the other hand, there are also certainly “shortcomings” in the obtained expressions which may at least partially inhibit their generalizability. For instance, once again, one would expect the impact of the presence of the 2nd soliton on the 1st to be the same as that of the first on the 2nd. In that sense, the equations on the first two lines do not reflect that reciprocity. The ones on the 3rd and 4th line seem to accurately reflect the dominant dynamics, but again (e.g., in the 4th line) there exists a potential shortcoming in that the greedy optimizer only identifies the dominant contribution to the phase dynamics, neglecting the exponentially weaker 2nd and 3rd terms in the 4th line of Eq. (2.6). While this does not appear to contribute significantly here, there may exist settings where such a term may play a more significant role. On balance, here we find that there is more room for potential improvement. The incorporation of physical attributes of the dynamics (such as the potential force reciprocity etc.) may enable further refinement of the dynamics identified. Nevertheless, we trust that this array of progressively more complex examples will be convincing to the reader of the potential value of utilizing such methods as a complement to existing techniques towards identifying the projections on the solitonic manifold (potentially even prior to seeking to analytically derive ones such).

5 Conclusions and future directions

In this work, we have revisited the time-honored problem of deriving effective equations for fundamental wave-like solutions of dispersive nonlinear partial differential equations, such as, notably, the bright and dark soliton solutions of the NLS equation. This so-called projection on the solitonic manifold and corresponding study of the resulting single-soliton and interaction dynamics of multiple solitons has been approached from a complementary data-driven perspective. While it is not inconceivable that such a data-driven approach

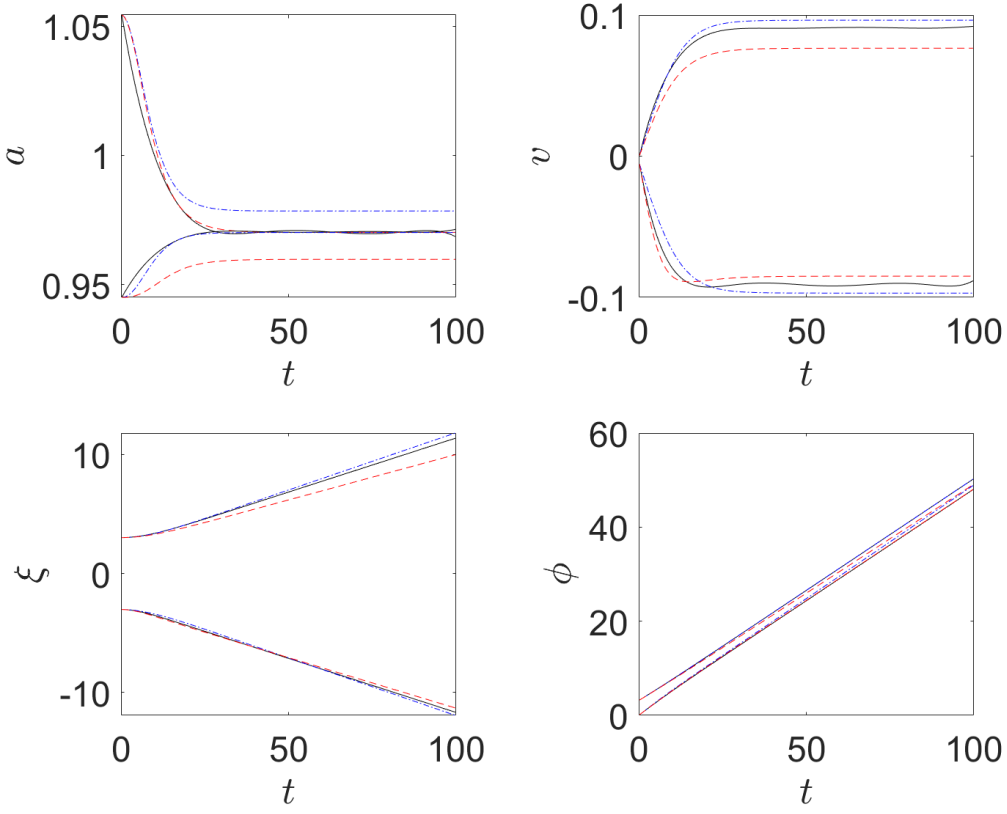


Figure 4: The comparison of the four soliton parameters in the four degrees of freedom system: we notice that in each panel above, the solid black, dashed red, and dashed-dotted blue curves depict the time-series data generated from the PDE simulation, the theoretical prediction based on system (2.6), and SINDy prediction based on the system (4.24) for each of the two solitons.

may yield results more accurate in special cases (yet, perhaps, often not as generalizable) as the traditional variational and asymptotic paper-and-pencil methods, its role here is intended to be complementing and perhaps guiding those, rather than replacing them. More specifically, in our considerations, we focused on identifying systems of ODEs that approximately govern the evolution of key characteristics of the solitonic waveforms. To this end, we employed the SINDy algorithm and its extension, SINDy with control, to learn the governing equations directly from time-series data. This was typically carried out for the position and velocity pair of conjugate variables, although some examples were also given of bright soliton cases where more variables (including amplitude and phase) were also involved.

Broadly speaking, our numerical experiments demonstrated that SINDy is capable of accurately recovering the theoretically derived reduced-order models for a variety of soliton interaction scenarios. However, we also observed limitations: in particular, the method could benefit from incorporation of physical principles such as the reciprocity of interactions between two solitons. Furthermore, the method showed reduced accuracy when applied to higher-dimensional systems, as illustrated in the multi-parameter, bright soliton case study presented in Subsubsection 4.3.4. This degradation in performance is likely attributed to the increased complexity of the underlying model (and the competition therein of multiple effects at different orders). Indeed, it is important to recognize the inherent challenges of applying sparse regression techniques in high-dimensional settings. Nevertheless, these limitations pose challenges that will be relevant to consider

in the future, possibly aided by more refined data-driven/machine learning tools.

In terms of the future directions, one possible avenue is to try to utilize alternative machine learning approaches such as the Neural Ordinary Differential Equations (Neural ODEs) [31] for dynamical equation identification when the reduced-order model has a relatively large dimensionality (e.g. see 4.3.4). Another direction is to extend the study of soliton interaction dynamics to some other mathematical physics models, such as the KdV equation mentioned in the introduction 1 and observe the outcomes therein. Indeed, upon amassing sufficient experience with known models (such as NLS, KdV, sine-Gordon etc.), one hopes to utilize this toolbox also in problems (possibly also higher-dimensional ones etc.) where such equations may not be analytically known. Additionally, while the current study focuses on interactions involving four or fewer solitons (Section 4), investigating the dynamics of larger soliton ensembles would provide a more rigorous test of the robustness of the techniques utilized herein. Although the underlying dynamics described by Eqs. (2.4) and (2.8) are expected to hold, such extended studies could further validate the consistency and scalability of data-driven model discovery. A number of these avenues is currently in progress and relevant results will be reported in future publications.

Acknowledgments

This material is based upon work supported by the U.S. National Science Foundation under the award PHY-2110030, PHY-2408988 and DMS-2204702 (P.G.K.) and DMS-2502900 (WZ) and by the Air Force Office of Scientific Research (AFOSR) under Grant No. FA9550-25-1-0079 (WZ). This research was partly conducted while P.G.K. was visiting the Okinawa Institute of Science and Technology (OIST) through the Theoretical Sciences Visiting Program (TSVP). This work was also supported by a grant from the Simons Foundation [SFI-MPS-SFM-00011048, P.G.K].

References

- [1] M. A. Ablowitz and P. A. Clarkson. *Solitons, Nonlinear Evolution Equations and Inverse Scattering*. London Mathematical Society Lecture Note Series. Cambridge University Press, 1991.
- [2] Mark J. Ablowitz and Harvey Segur. *Solitons and the Inverse Scattering Transform*. Society for Industrial and Applied Mathematics, 1981.
- [3] B. A. Malomed and P. G. Kevrekidis. Discrete vortex solitons. *Phys. Rev. E*, 64:026601, Jul 2001.
- [4] Panayotis G. Kevrekidis, Dimitri J. Frantzeskakis, and Ricardo Carretero-González. *The Defocusing Nonlinear Schrödinger Equation*. Society for Industrial and Applied Mathematics, Philadelphia, PA, 2015.
- [5] V.E. Zakharov and E.A. Kuznetsov. Multi-scale expansions in the theory of systems integrable by the inverse scattering transform. *Physica D: Nonlinear Phenomena*, 18(1):455–463, 1986.
- [6] Pierre Suret, Stephane Randoux, Andrey Gelash, Dmitry Agafontsev, Benjamin Doyon, and Gennady El. Soliton gas: Theory, numerics and experiments, 2023.
- [7] Manjun Ma, R. Navarro, and R. Carretero-González. Solitons riding on solitons and the quantum newton’s cradle. *Physical Review E*, 93(2), February 2016.
- [8] Wenlong Wang and P. G. Kevrekidis. Transitions from order to disorder in multiple dark and multiple dark-bright soliton atomic clouds. *Phys. Rev. E*, 91:032905, Mar 2015.
- [9] B. A. Malomed. Variational methods in nonlinear fiber optics and related fields. In E. Wolf, editor, *Progress in Optics*, volume 43, pages 71–193. Elsevier Science B.V., Amsterdam, The Netherlands, 2002.

[10] Ricardo Carretero-González, Dimitrios J. Frantzeskakis, and Panayotis G. Kevrekidis. *Nonlinear Waves & Hamiltonian Systems: From One To Many Degrees of Freedom, From Discrete To Continuum*. Oxford University Press, Oxford, United Kingdom, 2024.

[11] Gennady A El. Soliton gas in integrable dispersive hydrodynamics. *Journal of Statistical Mechanics: Theory and Experiment*, 2021(11):114001, nov 2021.

[12] Thibault Congy, Gennady El, and Giacomo Roberti. Soliton gas in bidirectional dispersive hydrodynamics. *Phys. Rev. E*, 103:042201, Apr 2021.

[13] Marcelo V. Flamarion, Efim Pelinovsky, and Ekaterina Didenkulova. Non-integrable soliton gas: The schamel equation framework. *Chaos, Solitons & Fractals*, 180:114495, 2024.

[14] Thibault Bonnemain and Benjamin Doyon. Soliton gas of the integrable boussinesq equation and its generalised hydrodynamics. *SciPost Physics*, 18(2), February 2025.

[15] Thibault Bonnemain, Benjamin Doyon, and Gennady El. Generalized hydrodynamics of the kdv soliton gas. *Journal of Physics A: Mathematical and Theoretical*, 55(37):374004, aug 2022.

[16] N.S. Manton. An effective lagrangian for solitons. *Nuclear Physics B*, 150:397–412, 1979.

[17] Yuri S. Kivshar and Boris A. Malomed. Dynamics of solitons in nearly integrable systems. *Rev. Mod. Phys.*, 61:763–915, Oct 1989.

[18] Yuri S. Kivshar and Wiesław Królikowski. Lagrangian approach for dark solitons. *Optics Communications*, 114(3):353–362, 1995.

[19] Boris A. Malomed. Potential of interaction between two- and three-dimensional solitons. *Phys. Rev. E*, 58:7928–7933, Dec 1998.

[20] D J Frantzeskakis. Dark solitons in atomic bose-einstein condensates: from theory to experiments. *Journal of Physics A: Mathematical and Theoretical*, 43(21):213001, may 2010.

[21] Paul K. Newton and George Chamoun. Vortex lattice theory: A particle interaction perspective. *SIAM Review*, 51(3):501–542, 2009.

[22] Hassan Aref. Point vortex dynamics: A classical mathematics playground. *Journal of Mathematical Physics*, 48(6):065401, 06 2007.

[23] Shuangquan Xie, Panayotis G. Kevrekidis, and Theodore Kolokolnikov. Multi-vortex crystal lattices in bose-einstein condensates with a rotating trap. *Proceedings of the Royal Society A: Mathematical, Physical and Engineering Sciences*, 474(2213):20170553, 2018.

[24] M. Konstantinov. Chaotic phenomena in the interaction of vortex rings. *Physics of Fluids*, 6(5):1752–1767, 05 1994.

[25] R. M. Caplan, J. D. Talley, R. Carretero-González, and P. G. Kevrekidis. Scattering and leapfrogging of vortex rings in a superfluid. *Physics of Fluids*, 26(9):097101, 09 2014.

[26] Jason H. V. Nguyen, Paul Dyke, De Luo, Boris A. Malomed, and Randall G. Hulet. Collisions of matter-wave solitons. *Nature Physics*, 10(12):918–922, 2014.

[27] A. Weller, J. P. Ronzheimer, C. Gross, J. Esteve, M. K. Oberthaler, D. J. Frantzeskakis, G. Theocharis, and P. G. Kevrekidis. Experimental observation of oscillating and interacting matter wave dark solitons. *Phys. Rev. Lett.*, 101:130401, Sep 2008.

[28] Chad R. Galley. Classical mechanics of nonconservative systems. *Phys. Rev. Lett.*, 110:174301, Apr 2013.

- [29] Weinan E. Dynamics of vortices in ginzburg–landau theories with applications to superconductivity. *Physica D: Nonlinear Phenomena*, 77(4):383–404, 1994.
- [30] Steven L. Brunton, Joshua L. Proctor, and J. Nathan Kutz. Discovering governing equations from data by sparse identification of nonlinear dynamical systems. *Proceedings of the National Academy of Sciences*, 113(15):3932–3937, March 2016.
- [31] Ricky T. Q. Chen, Yulia Rubanova, Jesse Bettencourt, and David Duvenaud. Neural ordinary differential equations, 2019.
- [32] M. Raissi, P. Perdikaris, and G.E. Karniadakis. Physics-informed neural networks: A deep learning framework for solving forward and inverse problems involving nonlinear partial differential equations. *Journal of Computational Physics*, 378:686–707, 2019.
- [33] J. Nathan Kutz, Steven L. Brunton, Bingni W. Brunton, and Joshua L. Proctor. *Dynamic Mode Decomposition*. Society for Industrial and Applied Mathematics, Philadelphia, PA, 2016.
- [34] Matthew O. Williams, Ioannis G. Kevrekidis, and Clarence W. Rowley. A data–driven approximation of the koopman operator: Extending dynamic mode decomposition. *Journal of Nonlinear Science*, 25(6):1307–1346, June 2015.
- [35] Urban Fasel, Eurika Kaiser, J. Nathan Kutz, Bingni W. Brunton, and Steven L. Brunton. SINDy with control: A tutorial, 2021.
- [36] Lev Pitaevskii and Sandro Stringari. *Bose-Einstein condensation and superfluidity*. International series of monographs on physics. Oxford University Press, Oxford, 2016.
- [37] Panayotis G Kevrekidis, Dimitri J Frantzeskakis, and Ricardo Carretero-González. *The defocusing nonlinear Schrödinger equation: from dark solitons to vortices and vortex rings*. SIAM, 2015.
- [38] Steven L. Brunton, Joshua L. Proctor, and J. Nathan Kutz. Discovering governing equations from data by sparse identification of nonlinear dynamical systems. *Proceedings of the National Academy of Sciences*, 113(15):3932–3937, 2016.
- [39] Stephen Billings. Nonlinear system identification: Narmax methods in the time, frequency, and spatio-temporal domains. *Nonlinear System Identification: NARMAX Methods in the Time, Frequency, and Spatio-Temporal Domains*, 08 2013.
- [40] M P Coles, D E Pelinovsky, and P G Kevrekidis. Excited states in the large density limit: a variational approach. *Nonlinearity*, 23(8):1753, jun 2010.
- [41] S. McEndoo and Th. Busch. Small numbers of vortices in anisotropic traps. *Phys. Rev. A*, 79:053616, May 2009.